Proton boron fusion reaction:

a novel experimental strategy for cross section investigation

D. Mazzucconi[a], D. Vavassori[a*], D. Dellasega[a], F. M. Airaghi[a], S. Agosteo[a], M. Passoni[a], A. Pola[a], D. Bortot[a]

[a] *Politecnico di Milano, Dipartimento di Energia, via La Masa 34, Milano, Italy*

ABSTRACT

The fusion reaction $^{11}B(p,\alpha)\alpha\alpha$ draws attention since the dawn of nuclear physics for its relevance and potential application in different fields, from nuclear fusion to astrophysics and hadron therapy. Nevertheless, the understanding and description of the physics of the reaction still have some important open points, both theoretical and experimental. Among others, the energy and angular distributions of α particles produced by the different reaction channels need to be further characterized, especially at low energies. To this aim, a novel experimental set-up was conceived by combining well-characterized boron-coated targets and a two-stage monolithic detection system. Targets were produced by Pulsed Laser Deposition, a technique that allows to finely tailor thickness, density and chemical composition of coatings. The detection system, based on a ΔE-E silicon telescope, was developed to perform an effective identification and discrimination between α particles produced by the p-^{11}B reaction and primary protons, essential for the reaction kinematic analysis at low energies. Irradiations were performed by bombarding a boron-coated foil with primary protons of energies in the range 1-2.4 MeV. Results show the effectiveness of the particle discrimination. Measured energy distributions highlight the contribution of α particles generated in the two main reaction channels. The reaction cross section was derived for each reaction channel at the different investigated energy and compared with literature data. The experimental set-up was also simulated through the Monte Carlo code FLUKA to test the model capabilities recently implemented in the code.

***Corresponding author**: Davide Vavassori; E-mail address: davide.vavassori@polimi.it

I. INTRODUCTION

The study of the $^{11}B(p, \alpha)\alpha\alpha$ reaction (hereinafter pB11) has been addressed since the dawn of nuclear physics, as evidenced by the pioneering experiments by Oliphant and Rutherford [1] and Gilbert and Dee [2]. In the last years, the research related to this reaction gained renewed interest, since it could be relevant for different research areas. Nowadays, the pB11 represents a potential candidate for the development of the so-called aneutronic fusion [3,4], a process that could avoid the issues related to the high neutron flux generated by the most commonly employed deuterium-tritium reaction. Moreover, pB11 is of interest both in nuclear astrophysics [5,6] and in nuclear reaction analysis [7]. More recently, the reaction has been proposed for the development of an enhanced proton therapy [8] and for the realization of α particles sources using high energy and high intensity lasers [9]. In this respect, to get a more comprehensive picture of the reaction, it is worth to briefly review which is the current understanding of the related physics and which are the main experimental approaches and results reported in previous works.

A. Reaction Physics

The present description of the physics of the reaction is based on a two-step process [10]. The proton, interacting with the ^{11}B nucleus, leads to the production of a $^{12}C^*$ compound nucleus in one of its highly excited states according to the incident proton energy. The decay of the $^{12}C^*$ nucleus is modelled as a sequence of a two breakup process in which the $^{12}C^*$ nucleus firstly produces a primary α particle and a ^{8}Be nucleus ($^{12}C^* \rightarrow \alpha_{prim} + {}^{8}Be$) that, in turn, breakups in two secondary α particles ($^{8}Be \rightarrow \alpha_{sec,1} + \alpha_{sec,2}$). Specifically, in the first step, the ^{8}Be nucleus can be produced in its ground state ($J^{\pi}=0^{+}$) or in its first excited state ($J^{\pi}=2^{+}$), which are referred as the α_0 channel and α_1 channel, respectively. Figure 1(a) shows the reaction scheme for some ^{12}C energy levels based on existing literature [11]. Analytical or experimental reaction cross sections that explicitly assume this scheme were also reported in literature [12, 13] or implemented in the Monte Carlo code FLUKA [14,15]. Figure 1(b) compares available results by highlighting the ^{12}C energy levels which should play a role (vertical lines). For proton energies in the range E_P = 0.1÷3 MeV, the reaction has been experimentally investigated and, using the two-step model, the breakup of different ^{12}C states (16.11, 16.62, 17.23, 17.76 and 18.38 MeV) has been described [10,12,16-36]. Nonetheless, some discrepancies and open points are still present. For example, as far as how the α_1 channel reaction proceed at the resonance E_P=0.675 MeV, a complete understanding of the break-up mechanism seems to be missing. Indeed, in more recent works, some authors report that the primary α particle should have orbital angular momentum l equal to 1 [30], while other authors report l=3 [33,34] or a mixture of the two [36] in agreement with the findings of previous works. Thus, it is evident that further efforts are needed for a complete comprehension of the reaction, also in view of the discussed applications. Specifically, the availability of reliable experimental data about fundamental quantities (e.g, cross section, α particle-proton ratio, α particle spectrum) is crucial. In this framework, the development of the experimental set-up is fundamental.

B. State-of-the-art

Experimental works focus on the measurement and analysis of α particle energy spectra. At $E_P \approx 0.1$ MeV, results show a sharp α peak around 6 MeV, assigned to the primary of α_0 channel, and a broad peak around 4 MeV, assigned to the primary of α_1 channel. Those values increase by increasing the energy of incident protons. This is the experimental evidence in the high-energy part of the measured α spectra. However, as already stressed in earlier works [21], if the low-energy part is considered, the interpretation is not so straightforward, due to the presence of protons elastically scattered by the target. To overcome this issue, some authors adopted multiple single-stage detectors in coincidence [10,19,21,32,35]. Results stress the presence of a contribution in the low-energy region associated to the secondary particles of the α_0 channel. Specifically, the coincidence spectrum measured by Laursen et al. [10] show a contribution in the low-energy region (1-2 MeV). According to the authors, this is originated by triple coincidence events mainly related to the α_0 channel. This is also in agreement with modelled spectra reported in [33,37]. Nevertheless, results obtained through coincidence techniques need to be integrated by further assessments of reaction cross sections.

An important role in the experimental investigation is played by the adopted boron targets. In previous works, boron targets are mainly produced by electron beam evaporation both as self-supporting foils and as films deposited over different kind of substrates (e.g., carbon, aluminium, tantalum, silver). In many cases, the target mass thickness, usually ranging from a few μg/cm^2 to a few 100s μg/cm^2, is only indirectly estimated during or after experiments. However, as underlined in [12,31], a proper characterization of the target thickness, but also of other properties such as density and chemical composition, is of relevance both to obtain accurate information and in view of simulation campaigns aimed to interpret measured data. Moreover, the exploitation of a different deposition technique that allows to vary considerably the mass thickness of the target, according to the physical quantity to be investigated, could represent a further step forward.

C. Concept of this work

A novel experimental set-up was conceived by combining a proper boron targets production and characterization strategy and a two-stage monolithic detection system. Targets are produced by Pulsed Laser Deposition, a technique that allows to finely tailor thickness, density and chemical composition of coatings. The detection system, based on a ΔE-E monolithic silicon telescope (MST), is developed to perform an effective physical identification and discrimination between α particles produced by the pB11 reaction and scattered protons, essential for the reaction kinematic analysis at low energies. The set-up is conceived to measure the whole energy spectrum of α particles to finely and directly characterize cross sections of the different reaction channels without any analytical assumptions or extrapolations.

In addition, the described experimental scheme was accurately reproduced and simulated using the Monte Carlo code FLUKA allowing both to optimize the proposed set-up and to compare the main features implemented in FLUKA related to the physics of the reaction with experimental results.

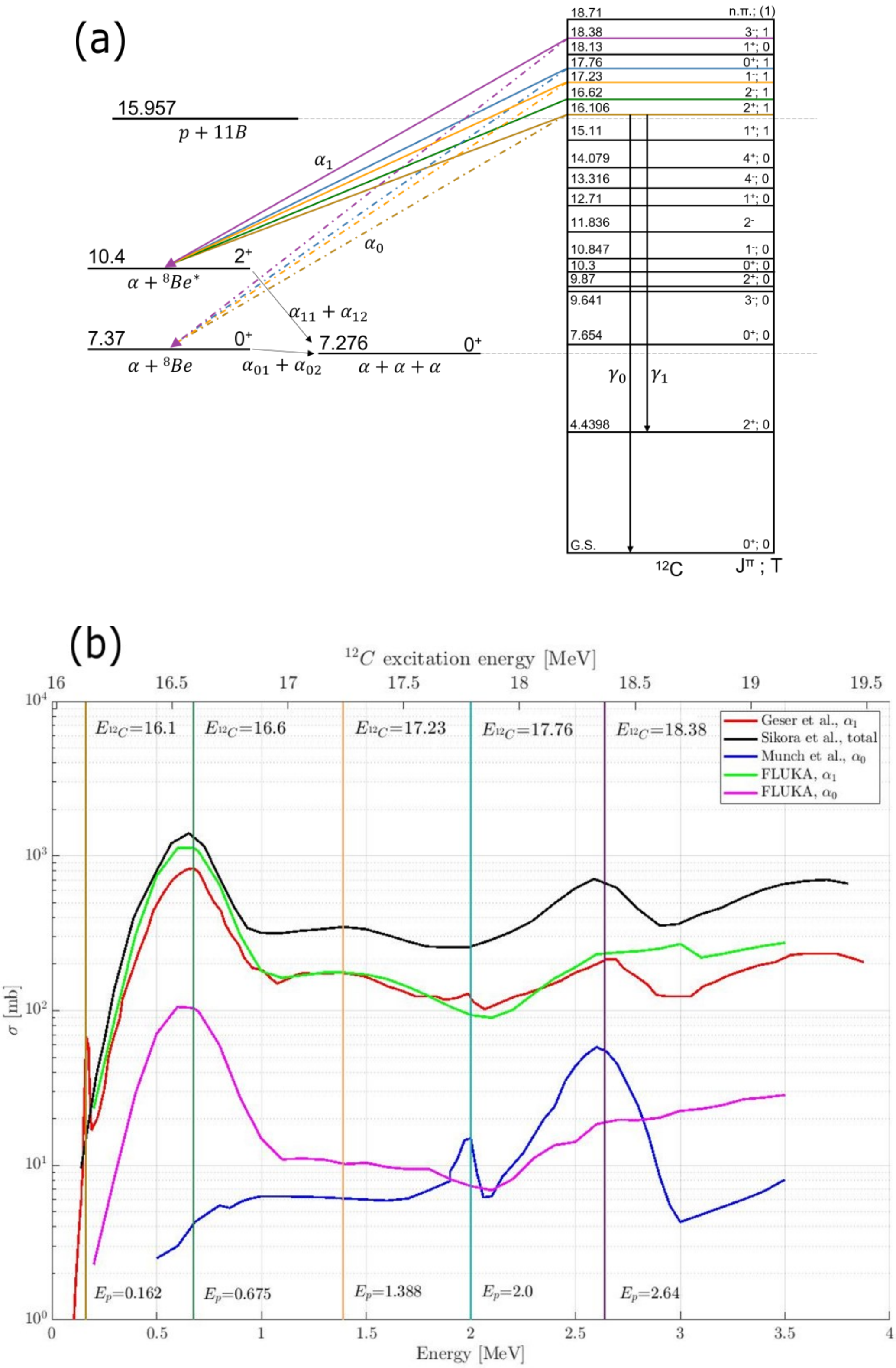

FIG.1. (a) The reaction scheme for five excited states of ^{12}C is shown. The arrows indicate the possible decay channel (α_0 or α_1) according to the conservation of angular momentum and parity. (b) The cross sections from some literature data are reported together with the cross sections extracted from FLUKA. The coloured lines indicate the energy of the ^{12}C excited states considered from the above scheme and the corresponding resonance energy for the reaction [11-13, 37].

II. MATERIALS AND METHODS

A. Boron targets

The selection of a proper target for a first experimental campaign was bound to the minimum proton energy delivered by the accelerator (see paragraph D in the present section), equal to 2 MeV. To have a lower proton energy at the boron layer, a low density 50 μm thick plastic substrate was considered. Therefore, boron (B) films have been deposited by Pulsed Laser Deposition (PLD) onto 50 μm thick PolyMethylMethAcrylate (PMMA) substrates and, for comparison and proper characterization, onto single side polished 500 μm thick (100) Si wafers. The adopted experimental setup is described in [38]. In all the depositions the background pressure was in the range $4÷6·10^{-3}$ Pa and the ablated target to substrate distance was set at 6 cm. The laser pulse energy varied between 735÷750 mJ, resulting in a laser fluence of 8.5 J/cm^2 (the laser spot area is assumed equal to 8.8 mm^2) and a deposition rate of about 70 nm/min. The morphological features were assessed by a Supra 40 Scanning Electron Microscope (SEM) with an accelerating voltage of 5 kV. SEM analyses of the B films deposited onto Si substrates are displayed in Figure 2(a) and 2(b). As already reported by Dellasega et al. [38], the film surface (Figure 2(a)) is quite smooth but due to the formation of molten droplets during the target ablation process, a certain number of micro and nanoaggregates are present. The cross-section SEM image (Figure 2(b)) shows a featureless amorphous morphology in which the previously mentioned film defects are clearly visible.

When the PMMA substrate is considered, the film surface (Figure 2(c)) results rougher and with and increased number of defects with respect to the films deposited on Si. At low magnification (Figure 2(d)), it can be observed that after the deposition the substrate surface is no longer flat, but it is characterized by the presence of corrugations and wrinkles on which the film is deposited. This is probably due both to a partial softening of PMMA during the deposition and to the high residual stress state associated to the amorphous B film. As a result, even for film thicknesses in the order of 100s of nm, the residual film stresses are sufficient to cause the PMMA substrate to roll up on itself. Thus, to overcome this problem, the scheme depicted in the left part of Figure 2(e) was adopted. By means of carbon adhesive tape, the PMMA substrate was framed inside an in-house made deposition double mask presenting a central square hole (2 cm x 2 cm) exhibiting the PMMA surface to be deposited. Exploiting this configuration, it was possible to keep the PMMA substrate flat and to obtain B targets as shown in the right part of Figure 2(e). Specifically, adjusting the deposition time, B films with an expected thickness of 1 μm and 5 μm were grown. The effective thickness, composition and density were assessed through the analysis of a silicon substrate inserted during the deposition on PMMA. Energy Dispersion X Ray Spectroscopy (EDXS) was performed to retrieve film composition. Density has been estimated using a quartz crystal microbalance (QCM), knowing the effective thickness evaluated through SEM cross section. The film properties are listed in Table I.

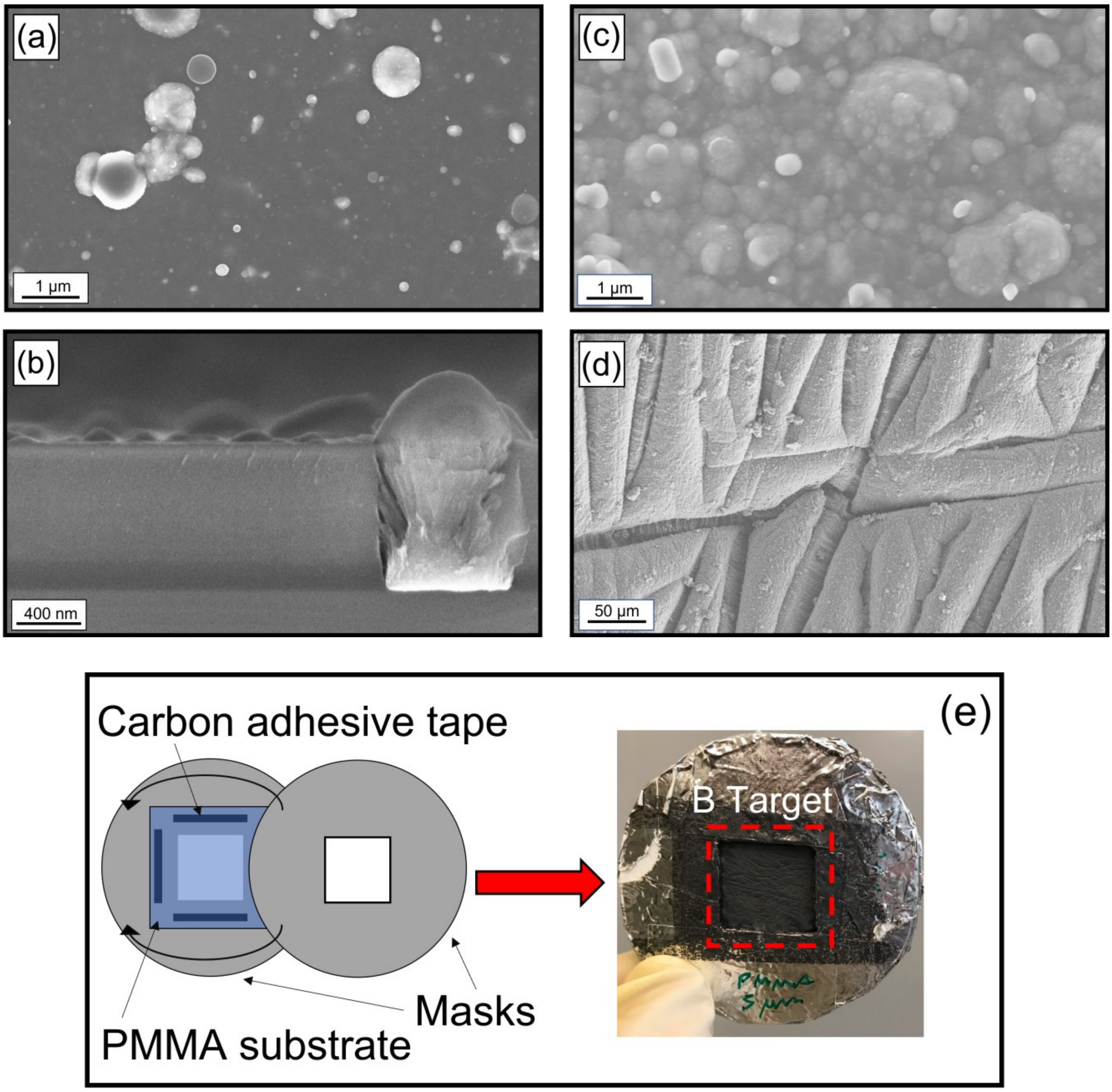

FIG. 2. SEM plane view (a) and cross section view (b) of B films deposited onto Si substrate. (c-d) SEM plane views of B films deposited onto PMMA substrate at different magnification. (e) The scheme adopted to keep the PMMA substrate flat (left) and the realized B target to be irradiated (right).

Expected Thickness [nm]	Effective Thickness [nm]	Atomic Fraction B O Mg	Density [g/cm³]	Mass Thickness [μg/cm²]
1000	900±40	82% 17% 1%	2.35 ± 0.2	211.84±27.44
5000	4580±150	86% 12% 2%		1078.04±127.1

TABLE I. Thickness, composition, density and mass thickness of deposited B films. Magnesium (Mg) is present as impurity in the ablated target.

B. The double-stage silicon telescope

The double stage detector adopted for the novel experimental set-up is based on a monolithic silicon telescope (MST). It is a layered silicon device constituted by a thin surface stage coupled to a deeper thick stage made out of the same wafer through deep ion implantation. The sketch of the device is shown in Figure 3. The two stages have a lateral extension of 1 mm^2. The first thin stage, 1.9 μm in thickness, provides an information strictly related to the stopping power of the impinging particle, while the second one, 500 μm in thickness, can measure the energy of the impinging particle [39,40]. Both stages, called ΔE and E, respectively, are collected separately by two different electronic chains. Signals are acquired by a two-channel ADC in coincidence mode to keep the time correlation between the E and ΔE events. The time resolution of the coincidence was 1 μs for minimizing the pile up probability (lower than 10^{-4}). The telescope allows to physically discriminate the type of the impinging particle by processing the bi-variate distribution of events, i.e. by elaborating the-so-called "ΔE-E scatter-plot".

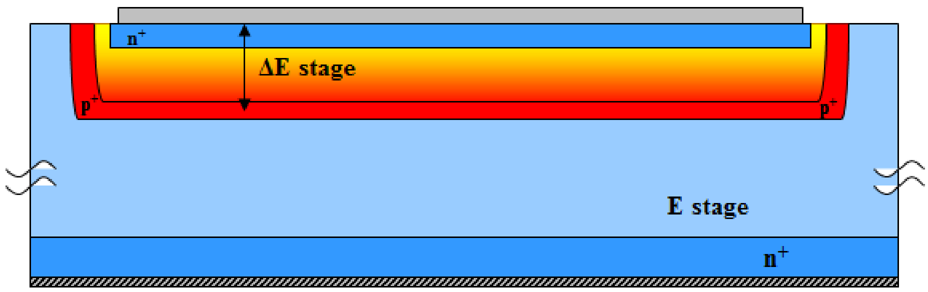

FIG. 3. Scheme of the monolithic silicon telescope.

The discrimination carried out by the silicon telescope offers the possibility of distinguishing, event-by-event, scattered protons from α particles generated in the pB11 reactions and, therefore, deriving spectra of α particles only.

C. Monte Carlo simulations of the p-^{11}B nuclear reaction

The Monte Carlo code FLUKA has recently introduced (since the 2020 release) the description of the pB11 reaction down to low energies. To date, FLUKA is a general-purpose Monte Carlo tool which implements the low energy reaction cross section and a complete transport of the generated α particles. The reaction cross section (for both channels) exploited by the code is plotted in Figure 1(b) compared with recent literature data [37].

FLUKA well reproduces the energy and the magnitude of the main reaction resonance at 675 keV, while it generally underestimates the reaction cross section for higher energies and it does not consider the other resonance at about 2.5 MeV. Moreover, the energy dependence of the α_0 channel cross section is similar to the total, being an order of magnitude lower. This is in contrast with data found by Spraker et al. [34] and Munch et al. [12], where the α_0 channel demonstrated at least 2 resonances at 2.64 and 3.5 MeV and a completely different spectral behavior. Nevertheless, the order of magnitude of the absolute value of the cross section, for energies greater than about 1 MeV, is on average in agreement with literature data summarized by Munch et al. [12].

Monte Carlo simulations were carried out for optimizing the experimental set-up to be exploited. In particular, the target with its composition and thickness and the silicon telescope were reproduced in detail in the code. The energy deposited in both stages of the detector by α particles and protons was scored to allow a comparison with experimental results.

D. Experimental set-up

The experimental campaign was carried out at the 7 MV CN Van de Graaff accelerator of the INFN – Laboratori Nazionali di Legnaro (LNL) in Legnaro, Italy. The targets and the silicon telescope were assembled on a specific plastic support, facing each other, and placed into a sealed vacuum chamber positioned along the 0° beamline of the accelerator. The accelerated proton beam was shaped with a circular aluminium collimator of 1 mm in diameter. Protons cross the target by interacting with the 50 μm PMMA substrate layer before reaching a boron target 900 nm in thickness. The silicon telescope was located at 60° with respect the beam direction. Accelerated proton energies were set equal to 2.1, 2.3, 2.8 and 3.1 MeV. The beam current (and the integral charge) was measured through a Faraday cup placed downstream of the target and connected to an electrometer. The configuration was adopted for maximizing the rate of the detected α particles for studying the reaction process. A scheme of this experimental set-up is reported in Figure 4(b).

The 50 μm PMMA layer was adopted to degrade the energy of accelerated protons, limited to a minimum value of 2 MeV by the accelerator. Energies that protons actually possess at the entrance of the boron target were calculated through Monte Carlo simulations that implements in detail the whole experimental set-up. More specifically, to be as close as possible to the experimental conditions, the actual proton energies at the entrance of the boron target were iteratively calculated to reproduce at best the distribution of scattered protons measured at 60° by the MST. From now on, proton energies will be referred at the boron surface as reported in Table II.

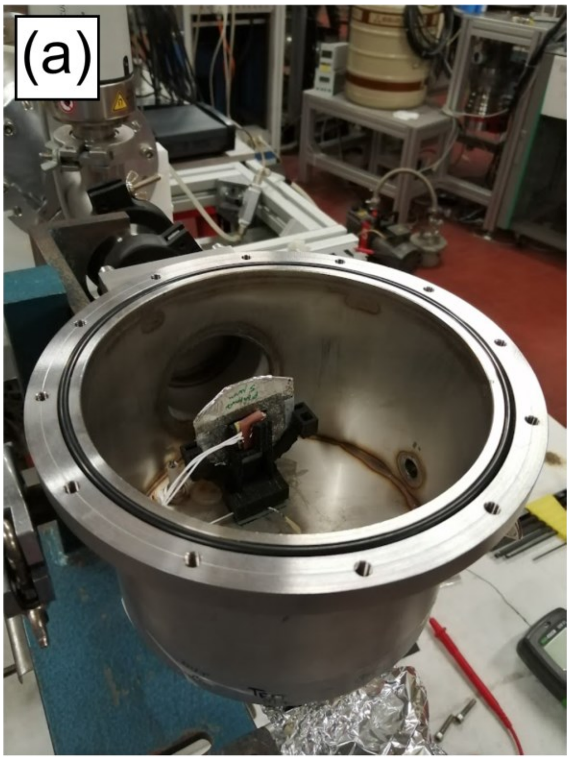

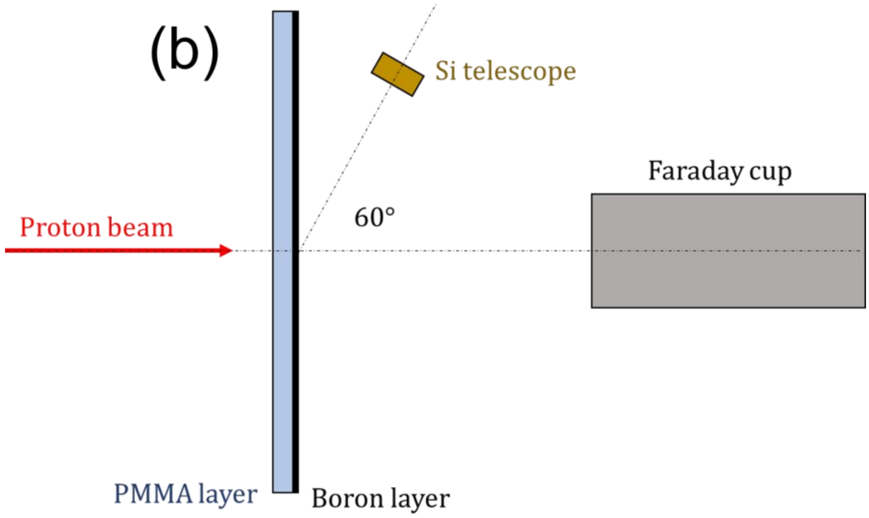

FIG. 4. (a) Picture of the experimental set-up. (b) Sketch of the experimental set-up.

Accelerated Proton Energy [MeV]	Average Proton Energy at the Boron Target [MeV]
2.1	1
2.3	1.3
2.8	2
3.1	2.4

TABLE II. Proton energies before and downstream the PMMA substrate.

III. RESULT AND DISCUSSION

The ΔE-E scatter-plots obtained in irradiations with 1.3 and 2.4 MeV protons are shown in Figure 5. As a reference, plots show the theoretical ΔE-E distribution of protons and α impinging normally on the device (red and black lines).

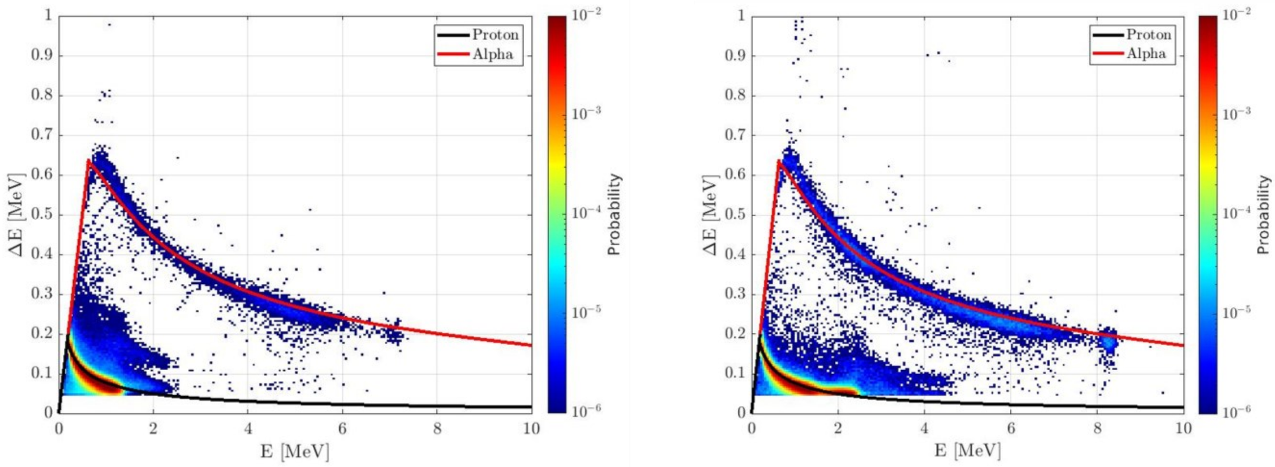

FIG. 5. Scatter-plots related to the proton and α signals. The two plots refer to 1.3 MeV (left side) and 2.4 MeV (right side) protons.

Two main contributions can be observed: protons elastically scattered by the target and its support (events around the black line) and α particles (events around the red line). The two populations are very well separated and therefore the energy spectra of α particles can be well discriminated from protons. Figure 6 shows α particle events selected through a non-linear discrimination threshold from scatter-plots of Figure 5. Using 2.4 MeV protons, in addition to the well-known high energy peaks around 8 and 6 MeV, a definite peak around 2 MeV is clearly visible.

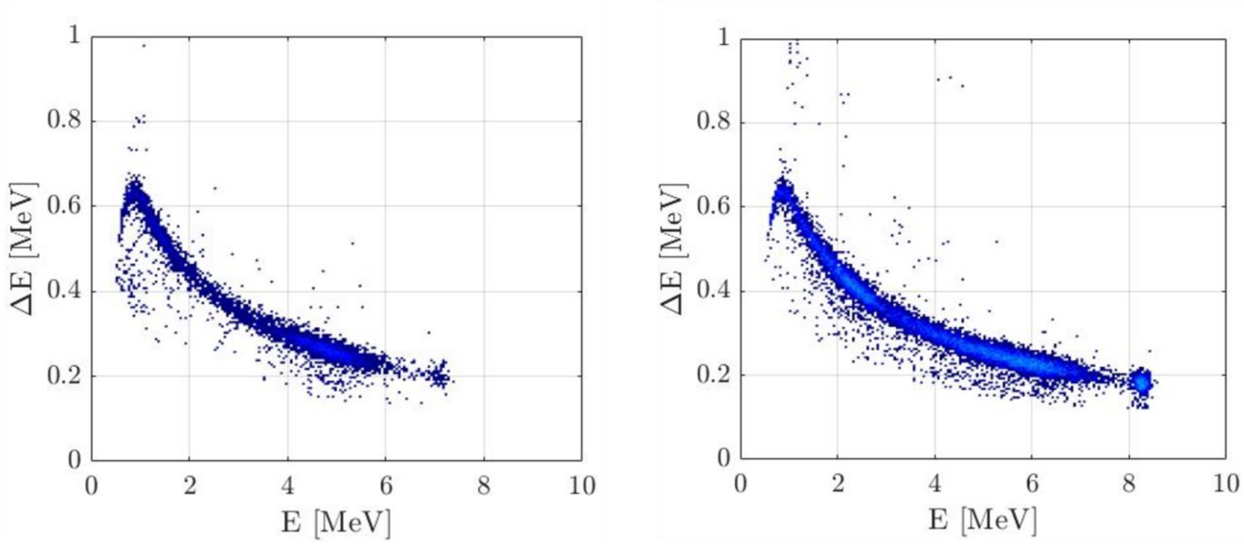

FIG. 6. Scatter-plots where the contribution of α particles only is shown. The two plots refer to 1.3 MeV (left side) and 2.4 MeV (right side) protons.

The benefit of using the MST is well represented in Figure 7, where energy spectra of α particles and scattered protons are plotted separately after the application of the discrimination procedure. If a single stage detector were used, many events pertaining to α particles would be hidden by scattered protons.

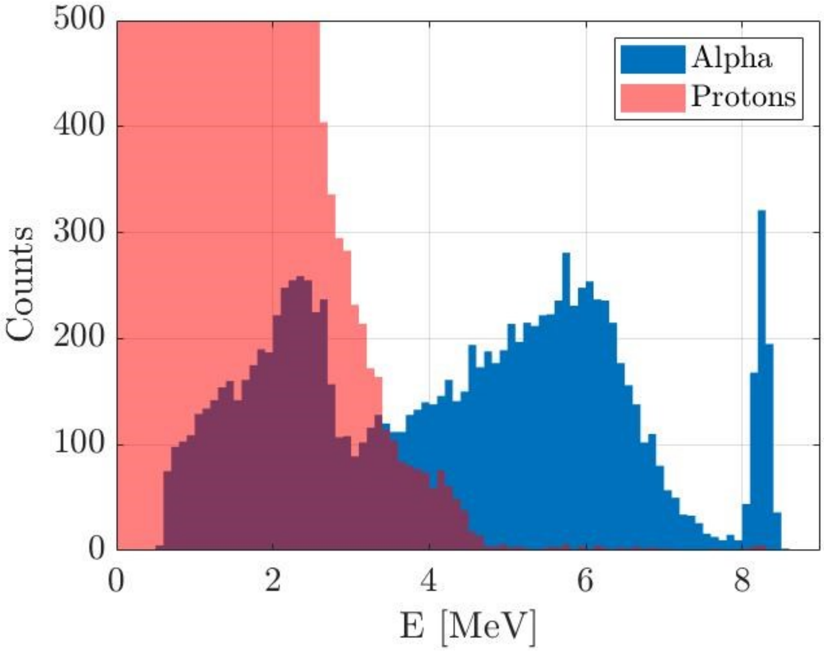

FIG. 7. Energy spectra of α particles and scattered protons after the application of the discrimination procedure (primary proton energy 2.4 MeV).

Alpha particles spectra measured at proton energies equal to 1, 1.3, 2 and 2.4 MeV are shown in Figure 8. All results highlight the presence of a main distribution peaked at an energy ranging from about 4.5 MeV to 6 MeV for proton energies from 1 MeV to 2.4 MeV, respectively. Values and behaviour of this distribution are consistent with α particles generated via the α_1 channel protons.

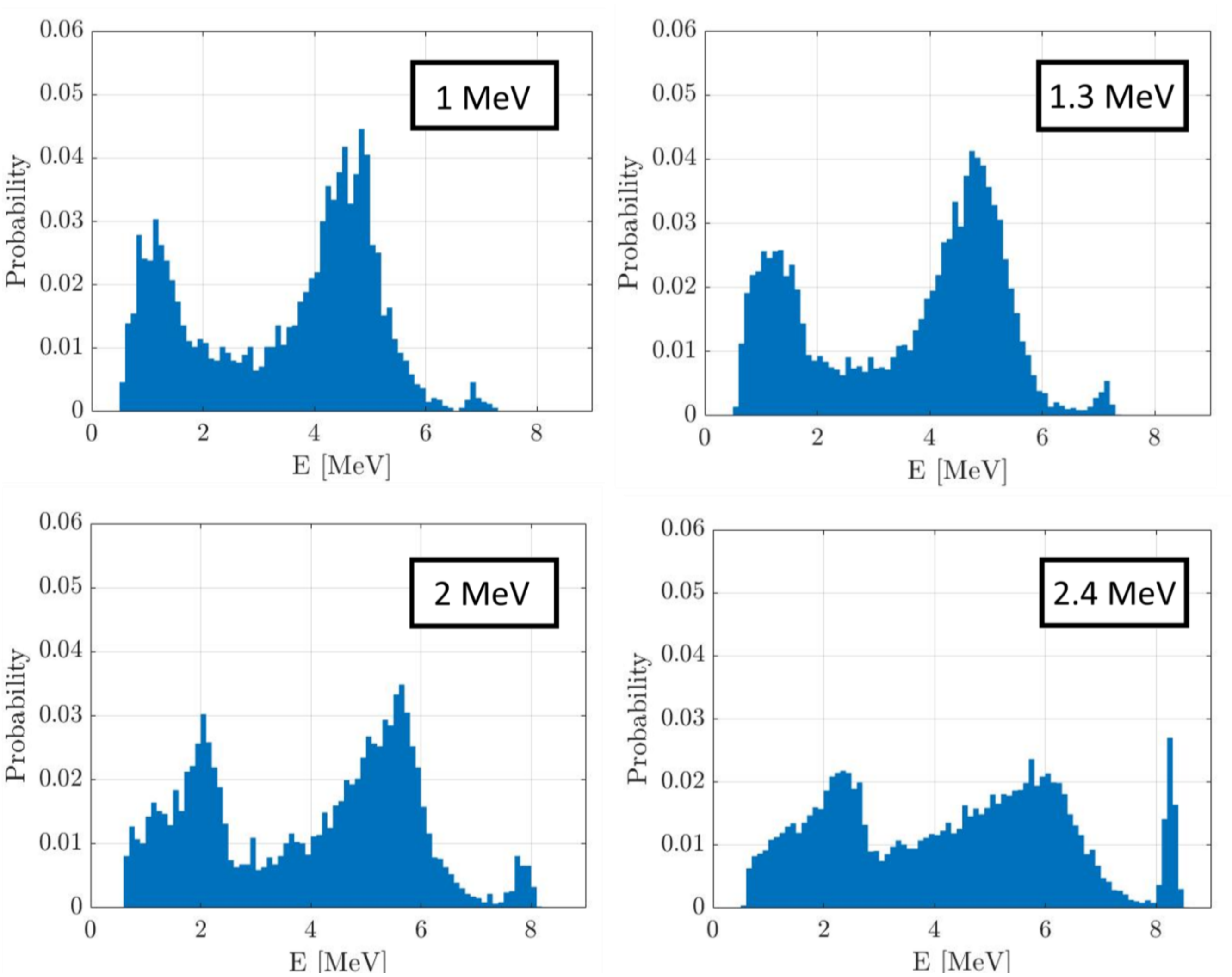

FIG. 8. Spectra of the measured α particles for different proton energies. The relative intensity of the different peaks depends on the beam energy.

All the energy spectra show two other contributions: a well-defined high energy peak, attributable to α particles from the α_0 channel, and a low-energy distribution, which becomes more evident for higher proton energies. The energies of the latter is compatible with secondary α particles emitted by the decay of the ^{8}Be nucleus (for both reaction channels) in agreement with previous models [32] and experimental results obtained with coincidence techniques [10]. It should be underlined that a single stage detector is not capable of measuring this distribution.

A preliminar quantitative analysis was carried out and reaction cross sections were assessed for the two different reaction channels. For both channels, the reaction cross section σ was computed as:

$$\sigma = 4\pi \frac{Counts}{N_t N_p d\Omega}$$

where N_t is the number of ^{11}B nuclei per cm^2 in the target, N_p is the number of incident protons, and dΩ is the solid angle subtended by the detector. Since measurements were performed at a unique position, for this preliminary calculation an isotropic emission of the α particles has been assumed.

The capability of the silicon telescope at discriminating α particles from protons allows the calculation of the reaction cross section by exploiting experimental data only, thus avoiding other assumptions. This approach is strongly different with other measurement techniques in which a single stage dectector is used. In those cases, a model is used to guess the low-energy part of α spectra (which fall under the scattered protons distribution) [37].

The calculation of the reaction cross section values at each energy was performed by processing measured spectra as follows:

- reaction cross section associated to the α_0 channel were derived by integrating counts under the well-defined high-energy peak, clearly separated from the remaining distribution.
- total reaction cross section (the sum of both channels) was evaluated by considering all measured counts related to α particles (i.e. integral counts of spectra in Figure 8).

The results obtained at the different proton energies are shown in Figure 9 together with literature data. Uncertainties are calculated by considering only counting statistics.

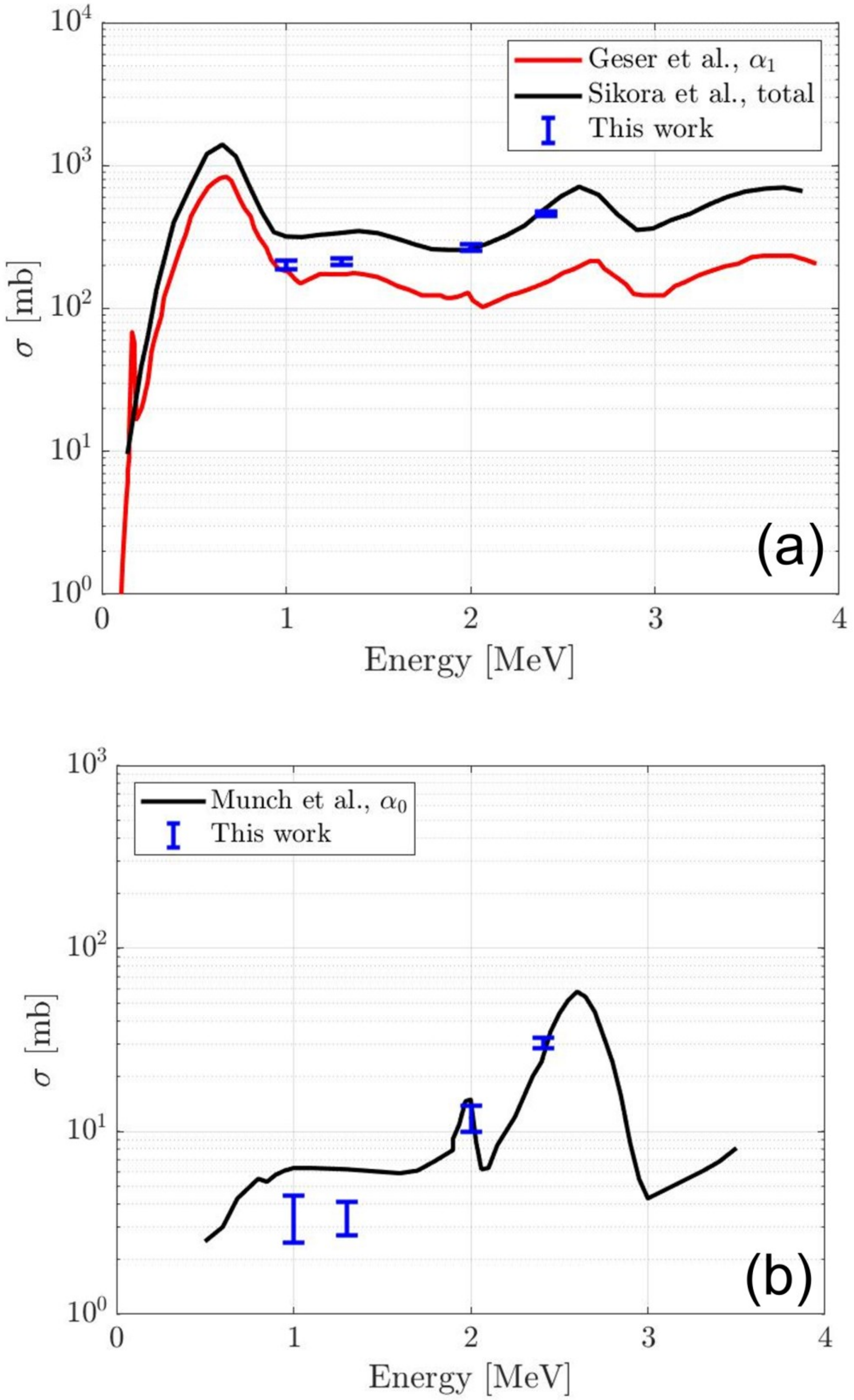

FIG. 9. (a) Total reaction cross section measured at different proton energies (blue) compared with data by Geser et al. (red) and Sikora et al. (black) [13,37]. (b) Reaction cross section for the α_0 channel (blue) compared with experimental data from Munch et al. (black) [12].

This preliminary comparison shows a good agreement between measurements and literature data for higher proton energies. In particular, the total reaction cross section values agree with results from Sikora et al. [37] at 2 and 2.4 MeV protons, while they differ at lower energies (1 and 1.3 MeV) (Figure 9(a)). The theoretical reaction cross section calculated by Geser et al. [13] for the α_1 channel (which is dominant for all the considered energies) is also shown. Figure 9(b) shows the comparison for the α_0 channel with data from [12]. The agreement is good for 2 and 2.4 MeV protons, while the results differ at 1 and 1.3 MeV .

Discrepancies at lower proton energies may be due to the thicknesses of substrate and target. As previously described, the first experimental configuration adopted for measurements employs a 900 nm boron target deposited onto a 50 μm PMMA. At low energies, straggling of primary protons introduces an energy spread from the accelerated value down to zero.

Results demonstrate, on the one hand, the performance of the novel experimental set-up proposed, while, on the other hand, allow to realize which actions can be implemented to improve the overall configuration. In particular, the effectiveness of the monolithic silicon telescope is confirmed, while there is the need of minimizing the thickness of the target substrate (maybe changing the material) and of the boron target.

As described in section II, all the experimental campaign was accurately reproduced by the FLUKA code. Numerical results were elaborated as the experimental ones for deriving the energy measured by the silicon telescope. As an example, the energy distribution of α particles transported by FLUKA for the proton energy equal to 1.3 MeV is compared to the experimental distribution in Figure 10.

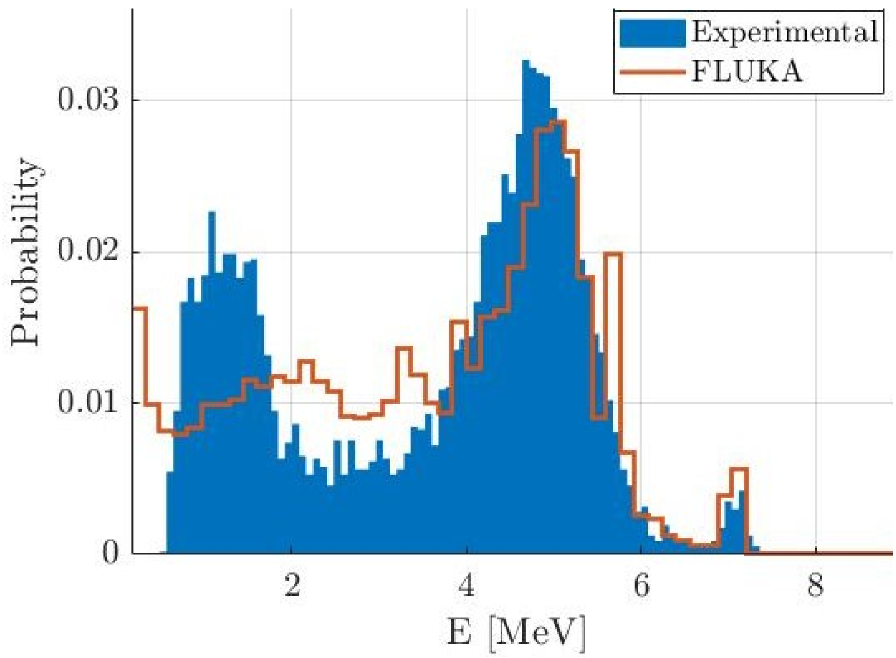

FIG. 10. Spectra of the measured α particles compared against FLUKA simulations for a proton energy equal to 1.3 MeV.

FLUKA reproduces quite well the general structure of the spectrum: energies of both the main peaks of the α_0 and α_1 channels are reproduced both in position and intensity. On the other hand, the trend for energies lower than the main α_1 peak show a clear discrepancy.

In spite of these partially controversial results, it is quite noticeable that a general purpose Monte Carlo tool like FLUKA generates and transports the α particles of both reaction channels with a quite reliable reaction cross section and kinematics. This will be certainly useful for future work and for the application of this code to innovative techiniques based on the proton-boron fusion reaction such as the Proton Boron Capture Therapy [8]. Certainly, the code will require some upgrades in terms of cross-sections and kinematics of the emitted α particles.

IV. CONCLUSIONS

A new experimental set-up based on a proper boron targets production and characterization and a double-stage monolithic silicon telescope was developed. Exploiting this strategy, it was possible to provide robust experimental data about the proton-boron fusion reaction for improving the study and the understanding of the related physics.

A first set of specific boron targets, properly tailored in thickness, density and chemical composition, were designed and developed for this purpose. These targets, constituted by a 900 nm boron layer deposited onto a 50 µm PMMA substrate, were irradiated with protons of energies between 1 and 2.4 MeV. Experimental results highlight the capability of the novel set-up of properly discriminating α particles generated by the fusion reaction from scattered primary protons. This capability allowed to derive energy distribution of α particles in the region typically overwhelmed by scattered protons.

Reaction cross sections at different proton energies were derived for the two different reaction channels. Values of the total reaction cross section and of the α_0 channel show a good agreement with literature data for 2 and 2.4 MeV protons. Some discrepancies were found for lower energies (1 and 1.3 MeV protons). These results suggest the need of an improvement of the target features to prevent proton beam straggling.

The simulation of the experimental set-up through the Monte Carlo code FLUKA highlights that the reaction cross section and the reaction kinematics implemented in the code needs further improvements. Nevertheless, a rather good description of the pB11 reaction in a general purpose tool like FLUKA widens the fields of applications of this reaction, from nuclear fusion to radiation therapy.

The results discussed in this work show that the novel experimental set-up is very promising and extremely useful for a comphensive approach to the characterization of pB11 reaction. After a target re-design and production, a systematic experimental campaigns based on a wider set of primary proton energies and angles will be performed.

ACKNOWLEDGMENTS

This work has been carried out within the framework of the EUROfusion Consortium, funded by the European Union via the Euratom Research and Training Programme (Grant Agreement No 101052200 — EUROfusion). Views and opinions expressed are however those of the author(s) only and do not necessarily reflect those of the European Union or the European Commission. Neither the European Union nor the European Commission can be held responsible for them.

References

[1] M. Oliphant, and L. Rutherford, Experiments on the transmutation of elements by protons, Proc. R. Soc. London. Ser. A, Contain. Pap. a Math. Phys. Character. 141 (1933) 259. https://doi.org/10.1098/rspa.1933.0117.

[2] P.I. Dee, and C.W. Gilbert, The disintegration of boron into three α-particles, Proc. R. Soc. London. Ser. A - Math. Phys. Sci. 154 (1936) 279. https://doi.org/10.1098/rspa.1936.0051.

[3] J.M. Dawson, (1981). Advanced fusion reactors. In Fusion (Teller, E., Ed.), Vol. 1, Part B, pp. 453-502, New York: Academic Press, (1981)

[4] F. Belloni, On a fusion chain reaction via suprathermal ions in high-density H–11B plasma, Plasma Phys. Control. Fusion. 63 (2021). https://doi.org/10.1088/1361-6587/abf255.

[5] Y. Yamashita, and Y. Kudo, Reaction mechanism of 11B(p, α) 8Be reaction at astrophysically relevant energies, Nucl. Phys. A. 589 (1995) 460–474. https://doi.org/10.1016/0375-9474(95)00069-D.

[6] L. Lamia et al.,, New measurement of the 11B(p,α0)8Be bare-nucleus S(E) factor via the Trojan horse method, J. Phys. G Nucl. Part. Phys. 39 (2012). https://doi.org/10.1088/0954-3899/39/1/015106.

[7] M. Kokkoris, A. Kafkarkou, V. Paneta, R. Vlastou, P. Misaelides, and A. Lagoyannis, Differential cross sections for the 11B(p,αo) 8Be and 11B(p,p0)11B reactions, suitable for ion beam analysis, Nucl. Instrum. Methods Phys. Res. Sect. B Beam Interact. with Mater. Atoms. 268 (2010) 3539–3545. https://doi.org/10.1016/j.nimb.2010.09.013.

[8] P. Bláha et al., The Proton-Boron Reaction Increases the Radiobiological Effectiveness of Clinical Low- and High-Energy Proton Beams: Novel Experimental Evidence and Perspectives, Front. Oncol. 11 (2021) 1–18. https://doi.org/10.3389/fonc.2021.682647.

[9] J. Bonvalet et al., Energetic α -particle sources produced through proton-boron reactions by high-energy high-intensity laser beams, Phys. Rev. E. 103 (2021) 1–11. https://doi.org/10.1103/PhysRevE.103.053202.

[10] K.L. Laursen, H.O.U. Fynbo, O.S. Kirsebom, K.S. Madsbøll,and K. Riisager, Complete kinematical study of the 3α breakup of the 16.11 MeV state in 12C, Eur. Phys. J. A. 52 (2016). https://doi.org/10.1140/epja/i2016-16271-2.

[11] J.H. Kelley, J.E. Purcell, and C.G. Sheu, Energy levels of light nuclei A = 12, Nucl. Phys. A. 968 (2017) 71–253. https://doi.org/10.1016/j.nuclphysa.2017.07.015.

[12] M. Munch, O.S. Kirsebom, J.A. Swartz, and H.O.U. Fynbo, Resolving the 11B (p, α) cross-section discrepancies between 0.5 and 3.5 MeV, Eur. Phys. J. A. 56 (2020) 1–7. https://doi.org/10.1140/epja/s10050-019-00016-8.

[13] F.A. Geser, and M. Valente, Analytical approach to the reaction cross section of the fusion of protons with boron isotopes aimed at cancer therapy, Appl. Radiat. Isot. 151 (2019) 96–101. https://doi.org/10.1016/j.apradiso.2019.04.034.

[14] T.T. Böhlen, F. Cerutti, M.P.W. Chin, A. Fassò, A. Ferrari, P.G. Ortega, A. Mairani, P.R. Sala, G. Smirnov, and V. Vlachoudis, The FLUKA Code: Developments and Challenges for High Energy and Medical Applications, Nuclear Data Sheets 120 (2014) 211-214.

[15] A. Ferrari, P.R. Sala, A. Fasso`, and J. Ranft, FLUKA: a multi-particle transport code, CERN-2005-10 (2005), INFN/TC_05/11, SLAC-R-773.

[16] O. Beckman, T. Huus, and A. Zupančič, Excitation curves for α particles from B11 bombarded with protons, Phys. Rev. 91 (1953) 606. https://doi.org/10.1103/PhysRev.91.606.

[17] G. Dearnaley, G.A. Dissanaike, A.P. French, and G. Lindsay Jones, Study of the B11+p reaction, Phys. Rev. 108 (1957) 743–753. https://doi.org/https://doi.org/10.1103/PhysRev.108.743.

[18] G.D. Symons, and P.B. Treacy, The B11 (p, α) Be8 reaction and C12 states between 15 and 20 MeV, Nucl. Phys. 46 (1963) 93–107. https://doi.org/10.1016/0029-5582(63)90567-4.

[19] D. Dehnhard, D. Kamke, and P. Kramer, Der Zerfall von Kohlenstoff 12 in drei α-Teilchen bei der Kernreaktion 11B(p,α) 2α, Ann. Phys. (1964). https://doi.org/10.1002/andp.19644690311.

[20] J.D. Bronson, W.D. Simpson, W.R. Jackson, and G.C. Phillips, Three α-particle decay of C12, Nucl. Phys. (1965). https://doi.org/10.1016/0029-5582(65)90643-7.

[21] D. Kamke, J. Krug, and F.W. Richter, Mechanism of the Reaction 11B(p, α)2α below and in the vicinity of the 675-keV resonance, Rev. Mod. Phys. 37 (1965) 453–454. https://doi.org/https://doi.org/10.1103/RevModPhys.37.453.

[22] R.E. Segel, S.S. Hanna, and R.G. Allas, States in C12 between 16.4 and 19.6 MeV, Phys. Rev. 139 (1965) B818. https://doi.org/10.1103/PhysRev.139.B818.

[23] D. Kamke, and J. Krug, Experimente zum Ablauf der Kernreaktion11B(p, 3α) in der 675 keV-Resonanz, Zeitschrift Für Phys. 201 (1967) 301–322. https://doi.org/10.1007/BF01326819.

[24] A. Giorni, D. Engelhardt, J.F. Cavaignac, J.P. Longequeue, and R. Bouchez, ETUDE DE LA REACTION A TROIS CORPS 11B(p,αα) α DE 150 keV A 2 MeV, Le J. Phys. 29 (1968) 4–8. https://doi.org/10.1051/jphys:019680029010400.

[25] J.L. Quebert, and L. Marquez, Effetts des résonaces de 12C sur l'émission de particules alpha dans la reaction B(p,3α), Nucl. Phys. A 126 (1969) 646–670.

[26] P.A. Treado, J.M. Lambert, V.E. Alessi, and R.J. Kane, Angular correlation and reaction mechanism for 11B(p,α)8Be2.9(α)4He with Ep < 1.4 MeV, Nucl. Phys. A. (1972). https://doi.org/10.1016/0375-9474(72)90769-5.

[27] Y. Chanut, J.N. Scheurer, R. Ballini, J.L. Quebert, Y. Flamant, and C. Perrin, Effets des spin et parité 3- de 12C (18.36 MeV) sur la répartition des énergies dans l'état final de la réaction 11B(p, 3α), Nucl. Phys. A. (1972). https://doi.org/10.1016/0375-9474(72)90999-2

[28] W. von Witsch, M. Ivanovich, D. Rendić, V. Valković, G.C. Phillips, and K. Schäfer, Decay of 12C via the 11B(p, 2α)α reaction, Nucl. Phys. A. (1972). https://doi.org/10.1016/0375-9474(72)90869-X.

[29] J.M. Davidson, H.L. Berg, M.M. Lowry, M.R. Dwarakanath, A.J. Sierk, and P. Batay-Csorba, Low energy cross sections for 11B(p, 3α), Nucl. Phys. A. 315 (1979) 253–268. https://doi.org/10.1016/0375-9474(79)90647-X.

[30] H.W. Becker, C. Rolfs, and H.P. Trautvetter, Low-Energy Cross Sections for, At. Nucl. 327 (1987) 341–355.

[31] J. Liu, X. Lu, X. Wang, and W.K. Chu, Cross-sections of 11B(p,α)8Be reaction for boron analysis, Nucl. Instrum. Methods Phys. Res. Sect. B Beam Interact. with Mater. Atoms. 190 (2002) 107–111. https://doi.org/10.1016/S0168-583X(01)01272-1.

[32] M. Bogovac, S. Fazinić, M. Jakšić, M. Lattuada, D. Miljanić, N. Soić, C. Spitaleri, and M. Zadro, 11B(p,αα)4He Reaction In Collinearity Configurations, Fiz. B. 4 (1995) 229–236.

[33] S. Stave, M.W. Ahmed, R.H. France, S.S. Henshaw, B. Müller, B.A. Perdue, R.M. Prior, M.C. Spraker, and H.R. Weller, Understanding the B11(p,α)αα reaction at the 0.675 MeV resonance, Phys. Lett. Sect. B Nucl. Elem. Part. High-Energy Phys. 696 (2011) 26–29. https://doi.org/10.1016/j.physletb.2010.12.015.

[34] M.C. Spraker et al., The 11B(p,α) 8Be → α + α and the 11B(α,α) 11B Reactions at Energies Below 5.4 MeV, J. Fus. Energy. 31 (2012) 357–367. https://doi.org/10.1007/s10894-011-9473-5.

[35] M. Munch, and H.O. Uldall Fynbo, The partial widths of the 16.1 MeV 2+ resonance in 12C, Eur. Phys. J. A. 54 (2018) 1–8. https://doi.org/10.1140/epja/i2018-12577-3.

[36] M. Kuhlwein, K. Lytje, H.O.U. Fynbo, A. Gad, E. Jensen, O.S. Kirsebom, M. Munch, J. Refsgaard, and K. Riisager, Exclusive decay study of the 16.62 MeV (2-, T=1) resonance in 12C, Phys. Lett. B 825 (2021) 136857. https://doi.org/10.1016/j.physletb.2021.136857.

[37] M.H. Sikora, and H.R. Weller, A New Evaluation of the 11 B(p, α) αα Reaction Rates, J. Fus. Energy. 35 (2016) 538–543. https://doi.org/10.1007/s10894-016-0069-y.

[38] D. Dellasega, V. Russo, A. Pezzoli, C. Conti, N. Lecis, E. Besozzi, M. Beghi, C.E. Bottani, and M. Passoni, Boron films produced by high energy Pulsed Laser Deposition, Mater. Des. 134 (2017) 35–43. https://doi.org/10.1016/j.matdes.2017.08.025.

[39] S. Agosteo, G.A.P. Cirrone, P. Colautti, G. Cuttone, G. D'Angelo, A. Fazzi, M.V. Introini, D. Moro, A. Pola, V. Varoli, Study of a silicon telescope for solid state microdosimetry: preliminary measurements at the therapeutic proton beam line of CATANA, Radiat. Meas. 45 (2010) 1284–9. https://doi.org/10.1016/j.radmeas.2010.06.051.

[40] D. Mazzucconi et al., Experimental investigation at CATANA facility of n-10B and p-11B reactions for the enhancement of proton therapy, Phys. Medica. 89 (2021) 226–231. https://doi.org/10.1016/j.ejmp.2021.08.008.